# Ordered Mesoporous Ni Nanowires with Enhanced Hydrogenation Activity Prepared by Electroless Plating on Functionalized SBA-15

Hui Li,[†] Hong Lin,[†] Songhai Xie,[‡] Weilin Dai,[‡] Minghua Qiao,[‡] Yufeng Lu,*[,§] and Hexing Li*[,†]

*Department of Chemistry, Shanghai Normal University, Shanghai 200234, China, Department of Chemistry, Fudan University, Shanghai 200433, China, and Chemical & Biomolecular Engineering Department, University of California, Los Angeles, California 90095*

*Received January 15, 2008. Revised Manuscript Received March 29, 2008*

Highly ordered mesoporous Ni nanowires were synthesized by Ni electroless plating on the amine-functionalized SBA-15 ($NH_2$−SBA-15) support, followed by removing the silica template with NaOH. The incorporation of amine groups into the pore channels and the subsequent activation of $NH_2$−SBA-15 with $PdCl_2$ acetone solution are essential for generating Pd crystal seeds distributed in the pore channels. As a result, the following Ni electroless plating occurred mainly in pore channels, leading to the formation of ordered Ni nanowires catalyst with high surface area, ordered mesopore arrangement, and higher activity than Raney Ni in liquid-phase *p*-chloronitrobenzene hydrogenation.

## Introduction

Mesoporous materials have attracted much attention because of their potential applications in adsorption, chromatography, gas storage, and catalysis.[1] To date, the compositions of mesoporous materials have expanded from silicas[2] to metal oxides,[3] metal sulfides,[4] metal phosphates,[5] and hybrid organosilicas.[6] Since the first report of mesoporous Pt in 1997,[7] a series of mesoporous metals have been synthesized by using a soft-templating method (e.g., surfactant-directed assembly).[8] However, the vigorous and often exothermic reduction of metal precursors usually damages the mesostructure of the soft template, leading to mesoporous metals with poor long-range order.[9] Adopting mesoporous silica as hard template was first introduced by Ryoo et al.,[10] which displays advantages in its specific topological stability, veracity, predictability and controllability.[11] Repetitive process of impregnations and $H_2$ reduction of metal precursor is necessary to full fill the mesoporous channels and microporous channels within the pore wall with metal,[9] which is essential to form an ordered mesoporous metallic replica. To date, only noble metals (e.g., Pt, Pd etc.) with mesoporous structure have been synthesized based on this method.[12] In viewpoint of practical applications, such as industrial catalysis, synthesis of low-cost non-noble metals

* To whom correspondence should be addressed. Tel: 86-21-64322272. Fax: 86-21-64322272. E-mail: hexing-li@shnu.edu.cn (H.L.); luucla@ucla.edu (Y.L.).
† Shanghai Normal University.
‡ Fudan University.
§ University of California, Los Angeles.

(1) (a) Kresge, C. T.; Leonowicz, M. E.; Roth, W. J.; Vartuli, J. C.; Beck, J. S. *Nature* **1992**, *359*, 710. (b) Beck, J. S.; Vartuli, J. C.; Roth, W. J.; Leonowicz, M. E.; Kresge, C. T.; Schmitt, K. D.; Chu, C. T. W.; Olsen, D. H.; Sheppard, E. W.; McCullen, S. B.; Higgins, J. B.; Schlenker, J. L. *J. Am. Chem. Soc.* **1992**, *114*, 10834.
(2) (a) Monnier, A.; Schüth, F.; Huo, Q.; Kumar, D.; Margolese, D.; Maxwell, R. S.; Stucky, G.; Krishnamurty, M.; Petroff, P.; Firouzi, A.; Janicke, M.; Chmelka, B. *Science* **1993**, *261*, 1299. (b) Huo, Q.; Margolese, D.; Ciesla, U.; Feng, P.; Gier, T.; Sieger, P.; Leon, R.; Petroff, P. M.; Ciesla, U.; Schüth, F.; Stucky, G. D. *Nature* **1994**, *368*, 317. (c) Huo, Q.; Margolese, D.; Ciesla, U.; Demuth, D.; Feng, P.; Gier, T.; Sieger, P.; Firouzi, A.; Chmelka, B.; Schüth, F.; Stucky, G. D. *Chem. Mater.* **1994**, *6*, 1176. (d) Tanev, P. T.; Chibwe, M.; Pinnavaia, T. J. *Nature* **1994**, *368*, 321. (e) Attard, G. S.; Glyde, J. C.; Göltner, C. G. *Nature* **1995**, *378*, 366. (f) Bagshaw, S. A.; Prouzet, E.; Pinnavaia, T. J. *Science* **1995**, *269*, 1242. (g) Zhao, D.; Feng, J.; Huo, Q.; Melosh, N.; Fredrickson, G. H.; Chmelka, B. F.; Stucky, G. D. *Science* **1998**, *279*, 548.
(3) (a) Antonelli, D. M.; Ying, J. Y. *Angew. Chem., Int. Ed.* **1995**, *107*, 2202. (b) Bagshaw, S. A.; Pinnavaia, T. J. *Angew. Chem., Int. Ed.* **1996**, *108*, 1180. (c) Yang, P.; Zhao, D.; Margolese, D. I.; Chemlka, B. F.; Stucky, G. D. *Chem. Mater.* **1999**, *11*, 2813. (d) Tian, Z. R.; Tong, W.; Wang, J. Y.; Duan, N. G.; Krishnan, V. V.; Suib, S. L. *Science* **1997**, *276*, 926. (e) Antonelli, D. M.; Ying, J. Y. *Angew. Chem., Int. Ed.* **1996**, *108*, 461.
(4) MacLachlan, M. J.; Coombs, N.; Ozin, G. A. *Nature* **1999**, *397*, 681.
(5) Ciesla, U.; Schacht, S.; Stucky, G. D.; Unger, K. K.; Schüth, F. *Angew. Chem., Int. Ed.* **1996**, *108*, 597.
(6) (a) Burkett, S. L.; Sim, S. D.; Mann, S. *Chem. Commun.* **1996**, 1367. (b) Macquarrie, D. J. *Chem. Commun.* **1996**, 1961. (c) Inagaki, S.; Guan, S.; Fukushima, Y.; Ohsuna, T.; Terasaki, O. *J. Am. Chem. Soc.* **1999**, *121*, 9611. (d) Asefa, T.; MacLachan, M. J.; Coombs, N.; Ozin, G. A. *Nature* **1999**, *402*, 867. (e) Inagaki, S.; Guan, S.; Ohsuna, T.; Terasaki, O. *Nature* **2002**, *416*, 304.
(7) Attard, G. S.; Göltner; C G.; Corker, J. M.; Henke, S.; Templer, R. H. *Angew. Chem., Int. Ed.* **1997**, *36*, 1315.
(8) (a) Attard, G. S.; Bartlett, P. N.; Coleman, N. R. B.; Elliott, J. M.; Wang, J. H. *Science* **1997**, *278*, 838. (b) Whitehead, A. H.; Elliott, J. M.; Owen, J. R.; Attard, G. S. *Chem. Commun.* **1999**, 331. (c) Nelson, P. A.; Elliott, J. M.; Attard, G. S.; Owen, J. R. *Chem. Mater.* **2002**, *14*, 524. (d) Bartlett, P. N.; Gollas, B.; Guerin, S.; Marwan, J. *Phys. Chem. Chem. Phys.* **2002**, *4*, 3835. (e) Luo, H. M.; Sun, L.; Lu, Y. F.; Yan, Y. S. *Langmuir* **2004**, *20*, 10218. (f) Yamuuchi, Y.; Momma, T.; Fuziwara, M.; Nair, S. S.; Ohsuna, T.; Terasaki, O.; Osaka, T.; Kuroda, K. *Chem. Mater.* **2005**, *17*, 6342. (g) Li, H. X.; Zhao, Q. F.; Wan, Y.; Dai, W. L.; Qiao, M. H. *J. Catal.* **2006**, *244*, 251. (h) Yamauchi, Y.; Ohsuna, T.; Kuroda, K. *Chem. Mater.* **2007**, *19*, 1335. (i) Li, H.; Yang, H. X.; Li, H. X. *J. Catal.* **2007**, *251*, 233.
(9) Tiemann, M. *Chem. Mater.* **2008**, *20*, 961.
(10) Ryoo, R.; Joo, S. H.; Jun, S. *J. Phys. Chem. B* **1999**, *103*, 7743.
(11) Tian, B. Z.; Liu, X. Y.; Yang, H. F.; Yu, C. Z.; Tu, B.; Zhao, D. Y. *Adv. Mater.* **2003**, *15*, 1370.
(12) (a) Kang, H.; Jun, Y. W.; Park, J. I.; Lee, K. B.; Cheon, J. *Chem. Mater.* **2000**, *12*, 3530. (b) Shin, H. J.; Ko, C. H.; Ryoo, R. *J. Mater. Chem.* **2001**, *11*, 260. (c) Shin, H. J.; Ryoo, R.; Liu, Z.; Terasaki, O. *J. Am. Chem. Soc.* **2001**, *123*, 1246. (d) Lee, K.; Kim, Y. H.; Han, S. B.; Kang, H.; Park, S.; Seo, W. S.; Park, J. T.; Kim, B.; Chang, S. *J. Am. Chem. Soc.* **2003**, *125*, 6844. (e) Chen, X. Y.; Lou, Z. Y.; Xie, S. H.; Qiao, M. H.; Yan, S. R. *Chem. Lett.* **2006**, *35*, 390.

10.1021/cm800790h CCC: $40.75 
Published on Web 05/23/2008

**Table 1. Electroless-Plating Bath Composition and Plating Conditions**

| | concentrations and conditions |
|---|---|
| $NiSO_4 \cdot 6H_2O$ | 0.1 mol/L |
| $NiCl_2 \cdot 6H_2O$ | 0.25 mol/L |
| $Na_3C_6H_5O_7 \cdot 2H_2O$ | 0.085 mol/L |
| $NaH_2PO_2 \cdot 2H_2O$ | 0.64 mol/L |
| $NH_4Cl$ | 2.0 mol/L |
| $Pb(NO_3)_2$ | $5 \times 10^{-3}$ mol/L |
| pH | 8.7 |
| temperature | 298 K |

are more preferable. However, repetitive impregnations and $H_2$ reductions could not fully fill the porous channels in silica template. Zhang et al. reported that the formation of Ni nanowires in SBA-15 mesoporous channels by electroless plating.[13] To confined the growth of metal outside the mesoporous channels, the external surface of the SBA-15 template was premodified with hydrophobic methyl group. However, the weak ion-exchange capability of silica surface resulted in the formation of mainly isolated Ni nanowires within the mesoporous channels.[13] Herein, we report a new approach to preparing mesoporous Ni nanowires with high surface area by electroless plating on a Pd-activated amine-functionalized SBA-15, followed by removing silica template. Such a Ni catalyst exhibits much higher activity than Raney Ni catalyst during liquid-phase *p*-chloronitrobenzene (*p*-CNB) hydrogenation.

## Experimental Procedures

**Material Preparation.** First, $NH_2$−SBA-15 support was synthesized by co-condensation of (3-aminopropyl)triethoxysilane (APTS) and tetraethyl orthosilicate (TEOS) with the molar ratio of 1: 9 in the presence of surfactant P123 as a template.[14] The surfactant and other organic residues were removed by refluxing in ethanol at 353 K for 24 h. Then, 0.60 g of the as-prepared $NH_2$−SBA-15 was added into 50 mL of acetone containing certain amount of $PdCl_2$. The solution was stirred at 298 K for 8 h, which ensured the complete coordination between $Pd^{2+}$ ions and $NH_2$ ligands in $NH_2$−SBA-15.[15] After being refluxed in dichloromethane for 14 h, the solid was centrifuged, washed thoroughly with dichloromethane, and dried in a vacuum at 298 K, followed by reduction with hydrogen flow at 573 K for 3 h to generate metallic Pd nanoparticles as crystal seeds.[16]

Electroless plating was carried out in 50 mL of aqueous solution with the composition and reaction condition modified from previous literature work[17] (see Table 1). In this plating process, $NiSO_4$ and $NiCl_2$ were used as the sources of metal ions; $NaH_2PO_2$ was used as a reducing agent; $Na_3C_6H_5O_7$ was used as a complexing agent for $Ni^{2+}$ in solution; $NH_4Cl$ was used as buffering agent for pH control; $Pb(NO_3)_2$ was used as an additive to stabilize the solution and improve the morphology of the nickel coating. The nickel plating process was based on the following redox reaction[17a]

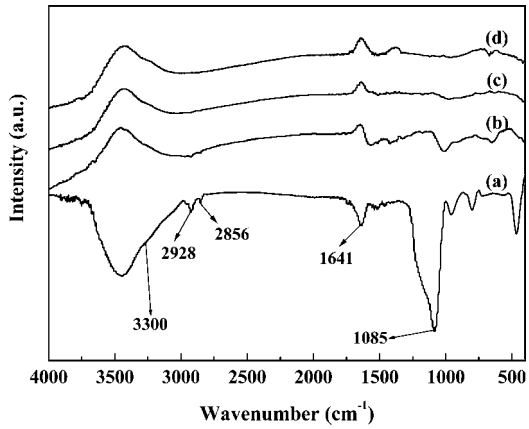


**Figure 1.** FTIR spectra of the (a) $NH_2$−SBA-15, (b) Ni-30-1, (c) Ni-30-2, and (d) Ni-30-3 samples.

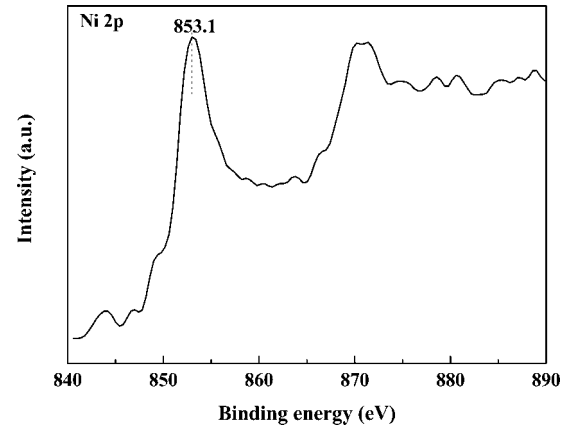


**Figure 2.** XPS spectrum of the Ni-30-2 sample.

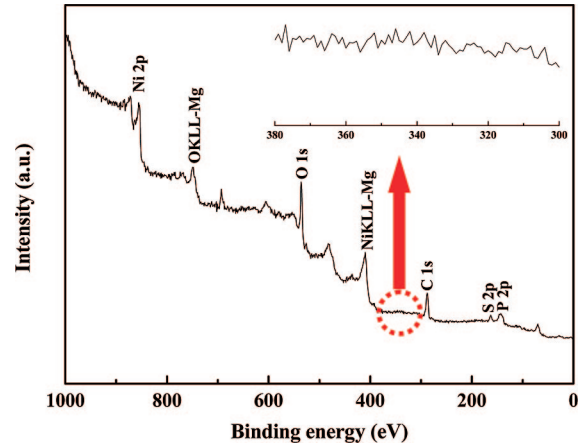


**Figure 3.** XPS survey spectrum of the Ni-30-2 sample.

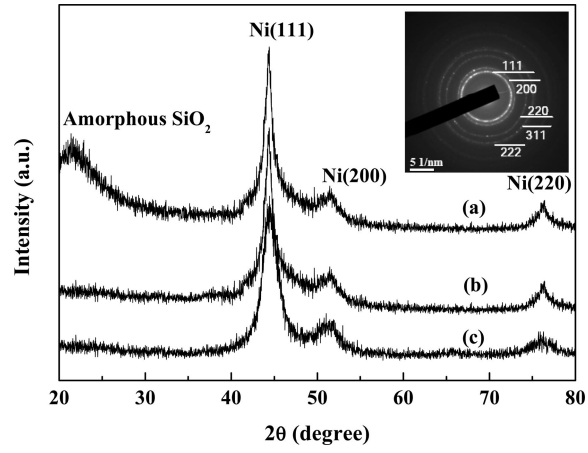


**Figure 4.** Wide-angle XRD patterns of (a) Ni/$NH_2$−SBA-15, (b) Ni-30-2, and (c) Raney Ni samples. The inset is the SAED image of the Ni-30-2 sample.

(13) Zhang, Z.; Dai, S.; Blom, D. A.; Shen, J. *Chem. Mater.* **2002**, *14*, 965.
(14) Chong, A. S. M.; Zhao, X. S. *J. Phys. Chem. B* **2003**, *107*, 12650.

$$\text{Cathodic reaction: } Ni_3(C_6H_5O_7)_2 + 6e^- \rightarrow 3Ni + 2C_6H_5O_7 \quad \text{(I)}$$

$$\text{Anodic reaction: } H_2PO_2^- + 3OH^- \rightarrow HPO_3 + 2H_2O + 2e^- \quad \text{(II)}$$

$$\text{Overall redox reaction: } Ni_3(C_6H_5O_7)_2 + 3H_2PO_2^- + 9OH^- \rightarrow 3Ni + 2C_6H_5O_7^{3-} + 3HPO_3^{2-} + 6H_2O \quad \text{(III)}$$

Because the standard reduction potential of the $Ni_3(C_6H_5O_7)_2$/Ni pair (−0.37 V vs standard hydrogen electrode, SHE) is higher than that of the $H_2PO_2^-/HPO_3^{2-}$ pair (−1.57 V vs SHE), $Ni^{2+}$ ions could be reduced into nickel by hypophosphite.[17a]

The silica template was removed by refluxing the silica/Ni composites in 250 mL of 4.0 M NaOH solution at 353 K for a certain time, followed by washing thoroughly with water until the pH reached 7. Finally, the solid was washed with ethanol (EtOH) three times and kept in EtOH until the time of use. The as-received sample is denoted as Ni-*x*-*y*, where *x* and *y* refer to the electroless plating time (minutes) and the etching time (days) in NaOH solution, respectively.

**Characterization.** The bulk composition was analyzed by inductively coupled plasma-optical emission spectroscopy (ICP-OES; Varian VISTA-MPX). $N_2$ adsorption−desorption isotherms were obtained at 77 K using a Quantachrome NOVA 4000e apparatus. Specific surface area ($S_{BET}$) was calculated by using the multiple-point Brunauer−Emmett−Teller (BET) method in the relative pressure range of $P/P_0 = 0.05-1.0$, and pore size distribution curve, together with average pore size ($D_p$) and pore volume ($V_p$), were obtained by the Barrett−Joyner−Halenda (BJH) model. Solid-state NMR ($^{29}$Si and $^{13}$C MAS NMR) spectra were obtained on a Bruker AV-400 NMR spectrometer. Fourier transform infrared (FTIR) spectra were recorded on a Nicolet Magna 550 spectrometer by KBr technique. X-ray powder diffraction (XRD) was carried out on a Rigaku D/Max-RB diffractometer with Cu*K*α radiation. Scanning electron microscopy (SEM) images were obtained using a JEOL JSM-6380LV microscope operating at 20 kV. Transmission electron microscopy (TEM) images were performed on a JEOL JEM2010 electron microscope at an acceleration voltage of 220 kV. X-ray photoelectron spectroscopy (XPS) measurements were performed on a Perkin-Elmer PHI 5000C ESCA system. All the binding energies were calibrated by using the contaminant carbon (C 1s = 284.6 eV) as a reference.

**Activity Test.** The hydrogenation of *p*-CNB was performed at 1.0 MPa $H_2$ and 353 K in a 200 mL stainless steel autoclave containing 0.40 g of Ni catalyst, 20 mmol of *p*-CNB, and 50 mL of EtOH. The reaction system was stirred vigorously (1000 rpm) to eliminate the diffusion effect. The reaction mixture was sampled at intervals for product analysis through a gas chromatograph (GC 9800) equipped with a flame ionization detector (FID) and an AC-5 column by using *n*-$C_{12}H_{25}OH$ as internal standard, from which reaction conversion and selectivity were calculated. The GC conditions are following: injector temperature, 513 K; oven temperature, programmed from 373 to 513 K at a ramping rate of 15 K/min; carrier gas $N_2$, 30 mL/min. Reproducibility was checked by repeating the runs at least three times and was found to be within acceptable limits (±A5%).

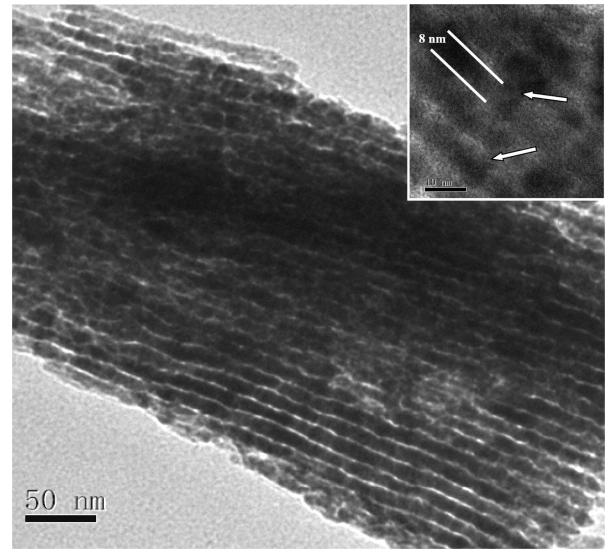


**Figure 5.** Representative TEM image of the Ni-30-2 sample. The inset is the HRTEM image. The arrows indicate the Ni nanopegs for fixing the Ni nanowires in an ordered arrangement.

## Results and Discussion

The $^{13}$C CP MAS NMR spectrum (see the Supporting Information, Figure S1) of $NH_2$−SBA-15 displays three well-resolved resonance peaks around 42.8, 21.1 and 9.2 ppm, corresponding to three carbon atoms in the $NH_2-CH_2-CH_2-CH_2$ group.[18] Meanwhile, the $^{29}$Si CP MAS NMR spectrum shows three upfield resonance peaks corresponding to $Q^4$ ($\delta = -109.8$), $Q^3$ ($\delta = -100.6$), $Q^2$ ($\delta = -91.0$) and two downfield peaks corresponding to $T^3$ ($\delta = -65.2$) and $T^2$ ($\delta = -57.2$), where $Q^n = Si(OSi)_n(OH)_{4-n}$ ($n = 2-4$) and $T^m = RSi(OSi)_m(OH)_{3-m}$ ($m = 1-3$).[19] From the FTIR spectra in Figure 1, one could see that $NH_2$−SBA-15 displays two bands at 2928 and 2856 $cm^{-1}$, characteristic of asymmetric and symmetric vibrations of C−H in the $NH_2-CH_2-CH_2-CH_2$ group.[20] Meanwhile, the absorbance band at 1641 $cm^{-1}$ indicative of N−H bending vibration is also clearly observed, though the $\upsilon_{N-H}$ vibration peak at 3300 $cm^{-1}$ is overlapped by O−H vibration at 3500 $cm^{-1}$.[18] These results confirm that $NH_2-CH_2-CH_2-CH_2$ group has been successfully incorporated into the pore channels of SBA-15. In comparison with Ni-30-1, both Ni-30-2 and Ni-30-3 samples display no signals indicative of the $NH_2-CH_2-CH_2-CH_2$ group. Even the absorbance bands at 1000−1130 and 1200−1250 $cm^{-1}$ indicative of Si−O and Si−C vibrations[21] disappear completely in either Ni-30-2 or Ni-30-3 sample. Thus, one could conclude that the $NH_2$−SBA-15 template has been completely removed after being treated in NaOH solution for 2 or 3 days, which could be further confirmed by EDX analysis (see the Supporting

(15) Shimazu, S.; Baba, N.; Ichikuni, N.; Uematsu, T. *J. Mol. Catal. A: Chem.* **2002**, *343*, 182–183.
(16) Hidber, P. C.; Helbig, W.; Kim, E.; Whitesides, G. M. *Langmuir* **1996**, *12*, 1375.
(17) (a) Mallory, G. O.; Hajdu, J. B. In *Electroless Plating: Fundamentals and Applications*; American Electroplaters and Surface Finishers Society: Orlando, FL, 1990; p 28. (b) Han, K. P.; Fang, J. L. J. *Appl. Electrochem.* **1996**, *26*, 1273. (c) Park, S. J.; Jang, Y. S.; Rhee, K. Y. *J. Colloid Interface Sci.* **2002**, *245*, 383.
(18) Huh, S.; Wiench, J. W.; Yoo, J.-C.; Pruski, M.; Lin, V. S.-Y. *Chem. Mater.* **2003**, *15*, 4247.
(19) Macquarrie, D. J.; Jackson, D. B.; Mdoe, J. E. G.; Clark, J. H. *New J. Chem.* **1999**, *23*, 539.
(20) Yang, C. M.; Sheu, H. S.; Chao, K. J. *Adv. Funct. Mater.* **2001**, *12*, 143.
(21) White, L. D.; Tripp, C. P. *Colloid Interface Sci.* **2000**, *232*, 400.

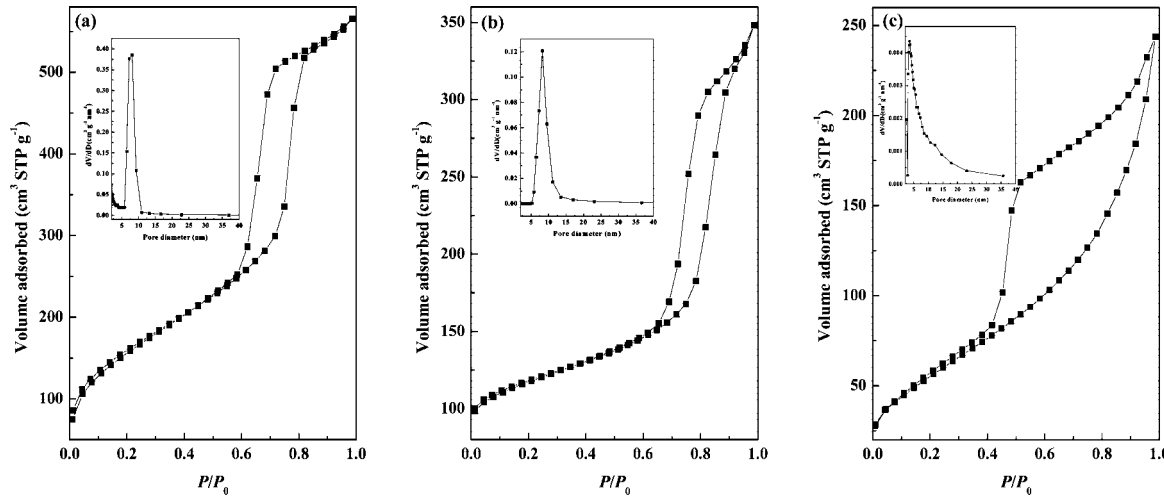


**Figure 6.** Adsorption/desorption isotherms of (a) $NH_2$−SBA-15, (b) Ni/$NH_2$−SBA-15, and (C) Ni-30-2 samples. The insets are the corresponding pore size distribution curves.

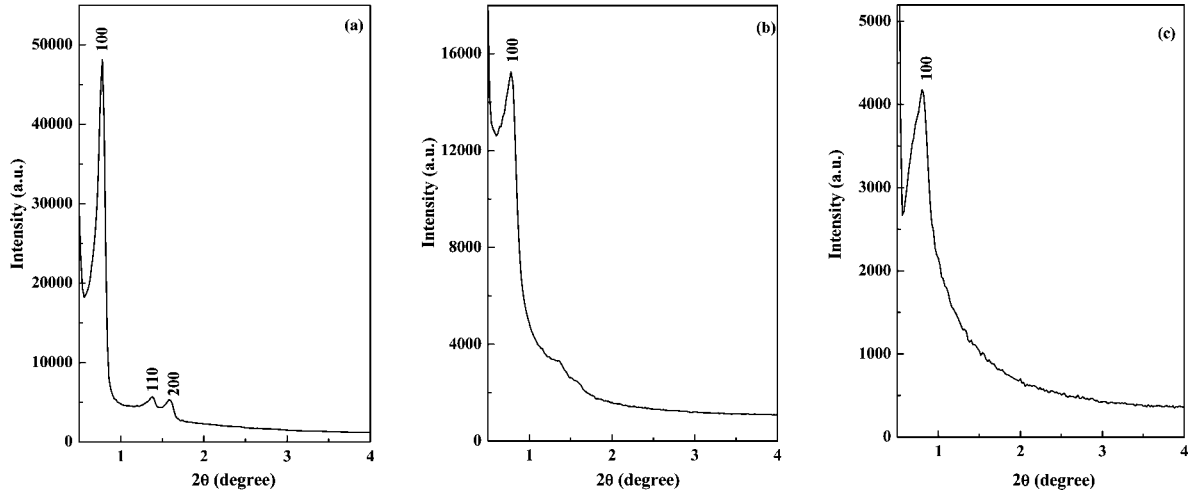


**Figure 7.** Low-angle XRD patterns of (a) $NH_2$−SBA-15, (b) Ni/$NH_2$−SBA-15, and (C) Ni-30-2 samples.

Information, Figure S2). The XPS spectrum (Figure 2) demonstrates that all the Ni species in the Ni-30-2 sample are present in the metallic state, corresponding to the binding energy of 853.1 eV in the Ni $2p_{3/2}$ level.[22] Because no XPS peaks indicative of Pd species are observed (Figure 3), it could be concluded that no significant amount of Pd species are present on the outer surface of the final product. Moreover, the XPS survey spectrum also reveals that the as-prepared Ni-30-2 contains some contaminants, including C, O, P, and S. The C 1s peak is probably due to the surface contaminant carbon. The O 1s peak is maybe related to the presence of oxides, such as phosphorus oxide. The presence of P species is inevitable, because the reactions for nickel plating produce phosphorus in both the oxidized state and alloying state with Ni.[17a]The presence of S 2p could be attributed to the inclusion of $SO_4^{2+}$ in the deposit.[17b] As shown in Figure 4, both Ni/$NH_2$−SBA-15 and Ni-30-2 samples display high-angle XRD patterns similar to those of Raney Ni with well-resolved crystalline diffraction peaks characteristic of Ni(111), Ni(200), and Ni(220), which could be further confirmed by the attached SAED image.[23] In comparison with Ni/$NH_2$−SBA-15, the broad peak around $2\theta = 22°$ indicative of amorphous $SiO_2$[24] disappears totally in Ni-30-2, suggesting that $NH_2$−SBA-15 template has been completely removed by NaOH etching for 2 days. This is consistent with the conclusion drawn from FTIR spectra.

The TEM morphology and the attached HRTEM image (Figure 5) demonstrate that Ni-30-2 is present in the form of nanowires with the average diameter around 8.0 nm, almost the same as the pore diameter of $NH_2$−SBA-15.[25] These Ni nanowires are fixed in ordered arrangement via thinner Ni nanowires, known as nanopegs.[9] Figure 6 reveals that both $NH_2$−SBA-15 and Ni/$NH_2$−SBA-15 samples display well-defined type IV $N_2$ adsorption−desorption isotherms with H1 hysteresis indicative of two-dimensional hexagonal mesoporous structure.[26] Although the isotherm

(22) Salvati, L.; Makovsky, L. E.; Stencel, J. M.; Brown, F. R.; Hercules, D. M. *J. Phys. Chem.* **1981**, *85*, 3700.
(23) Bao, J. C.; Liang, Y. Y.; Xu, Z.; Si, L. *Adv. Mater.* **2003**, *15*, 1832.
(24) Rioux, R. M.; Song, H.; Hoefelmeyer, J. D.; Somorjai, G. A. *J. Phys. Chem. B* **2005**, *109*, 2192.
(25) Wan, Y.; Zhang, F.; Lu, Y. F.; Li, H. X. *J. Mol. Catal. A: Chem.* **2006**, *267*, 165.
(26) Gregg, S. J.; Sing, K. S. W. *Adsorption, Surface Area and Porosity*; Academic Press: New York, 1982.

**Scheme 1**

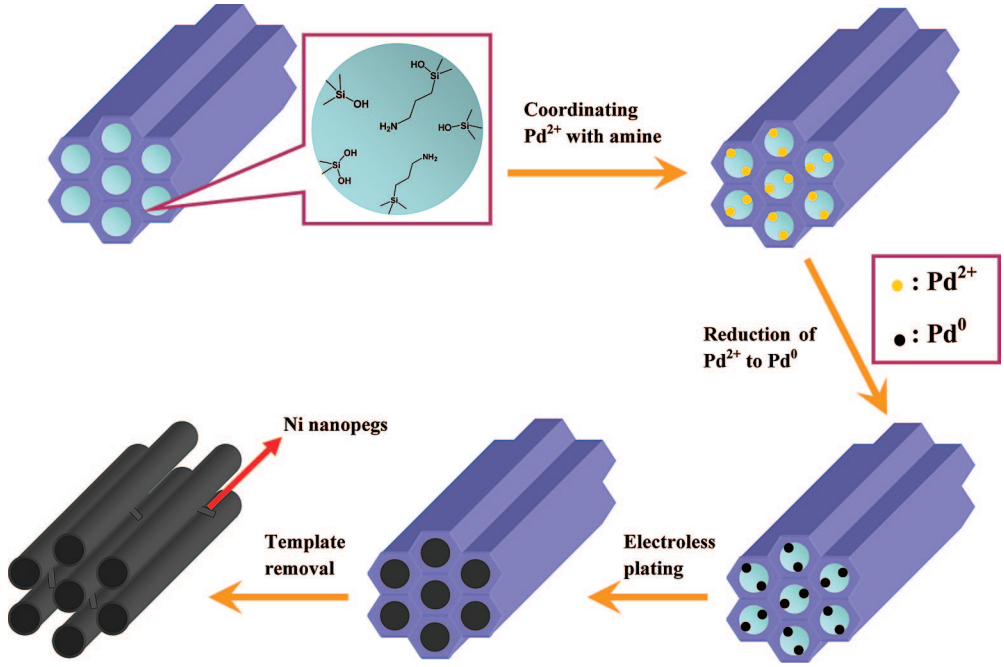


of Ni-30-2 shows a significant reduction in nitrogen uptake relative to $NH_2$−SBA-15 because of an increase in the scaffold density, a type IV isotherm is still observed for Ni-30-2 with a similar shape to those observed for other mesoporous transition metal oxides formed by hard templating.[27] Ni-30-2 displays a narrow pore size distribution (calculated from the adsorption isotherm) centered around 3.5 nm, which is similar to the wall thickness of NH $_2$-SBA-15 (4.1 nm).[25] These results demonstrate that the mesoporous structure of SBA-15 is successfully replicated in Ni-30−2. The low-angle XRD patterns in Figure 7 further confirm that both Ni/$NH_2$−SBA-15 and Ni-30−2 reserve the mesoporous structure in $NH_2$−SBA-15, corresponding to a well-resolved peak around $2\theta = 0.8°$ that is indicative of (100) diffraction.[2] The reduced peak intensity and the disappearance of two small peaks indicative of (110) and (200) diffractions[2] imply a lower ordering degree of the mesoporous structure.

Scheme 1 schematically illustrates the formation of ordered mesoporous Ni nanowires. The Pd(II) ions first coordinate with the $NH_2$ ligands linked on the mesoporous channels of $NH_2$−SBA-15 template and are then reduced into metallic Pd nanoparticles. These Pd nanoparticles then act as crystal seeds, promoting the growth of metallic Ni inside the pore channels. Removal of the $NH_2$−SBA-15 template results in Ni nanowires with an average diameter similar to the pore size of $NH_2$−SBA-15. These Ni nanowires are fixed in ordered arrangement by Ni nanopegs formed within the microporous pore wall in the $NH_2$−SBA-15.[27b] The mesopores formed between the Ni nanowires could be considered as the pore wall of $NH_2$−SBA-15, which is dissolved in NaOH solution. As a result, the average pore size in Ni-30-2 is similar to the wall thickness of the $NH_2$−SBA-15 template. The decrease in ordering degree could be mainly attributed to the damage of mesoporous channels during etching $NH_2$−SBA-15 in NaOH solution. In the absence of $NH_2$ groups, only sheetlike Ni could be obtained (see the Supporting Information, Figure S3). Meanwhile, activation of $NH_2$−SBA-15 with a suitable number of Pd crystal seeds is also essential for achieving ordered mesoporous Ni nanowires (Figure 8a). In the absence of Pd activation, only Ni nanoparticles deposited on the outside surface of $NH_2$−SBA-15 support were observed, corresponding to randomly dispersed Ni nanoparticles after removing the template (Figure 8b). However, activation of $NH_2$−SBA-15 with excess Pd leads to the formation of thin Ni film covering the surface of $NH_2$−SBA-15 during Ni electroless plating (Figure 8c) due to the presence of high-density Pd crystal seeds on the outer surface.

The role of the plating time is illustrated in Figure 9. Ni-10-2 displays Ni nanorods because the pore channels of $NH_2$−SBA-15 could not be completely filled by Ni within the short plating time (10 min). Because no Ni nanopegs are formed in the side-micropores of $NH_2$−SBA-15, these Ni nanorods could not be fixed in ordered arrangement. Thus, only randomly dispersed Ni nanorods have been found in the TEM image. Ni-20-2 shows mesoporous Ni nanowires owing to the full filling of metal Ni in mesoporous channels of $NH_2$−SBA-15 after Ni electroless plating for 20 min. However, the plating time is still not long enough to fill Ni in the side micropores of $NH_2$−SBA-15. Thus, these Ni nanowires could not be fixed in ordered arrangement due to the absence of Ni nanopegs. Ordered mesoporous Ni nanowires are obtained at plating time of 30 min owing to the complete filling of metal Ni in both the mesoporous and the side-microporous channels of $NH_2$−SBA-15 (see Figure 5). Besides the plating time, the etching time in NaOH solution is also important for obtaining ordered mesoporous Ni nanowires. As confirmed by aforementioned FTIR (Figure

(27) (a) Jiao, F.; Harrison, A.; Jumas, J. C.; Chadwick, A. V.; Kockelmann, W.; Bruce, P. G. *J. Am. Chem. Soc.* **2006**, *128*, 5468. (b) Dickinson, C.; Zhou, W.; Hodgkins, R. P.; Shi, Y.; Zhao, D.; He, H. *Chem. Mater.* **2006**, *18*, 3088.

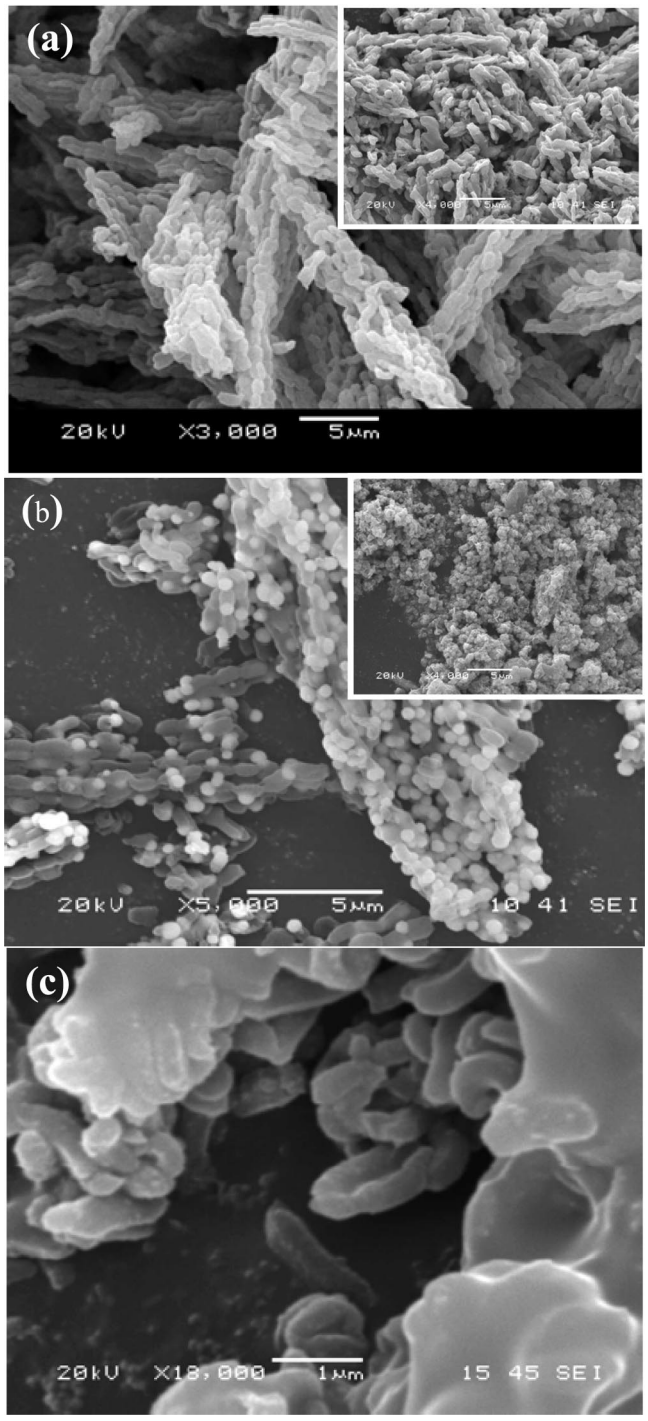


**Figure 8.** Effect of Pd content used for activating $NH_2$−SBA-15 on the SEM morphologies of the Ni/$NH_2$−SBA-15 obtained by Ni electroless plating for 30 min: (a) 0.0048, (b) 0, and (c) 0.018 g. The inset in (a) is the SEM image of the $NH_2$−SBA-15 template. The inset in (b) is the SEM image of the corresponding Ni sample after removal of the $NH_2$−SBA-15 template.

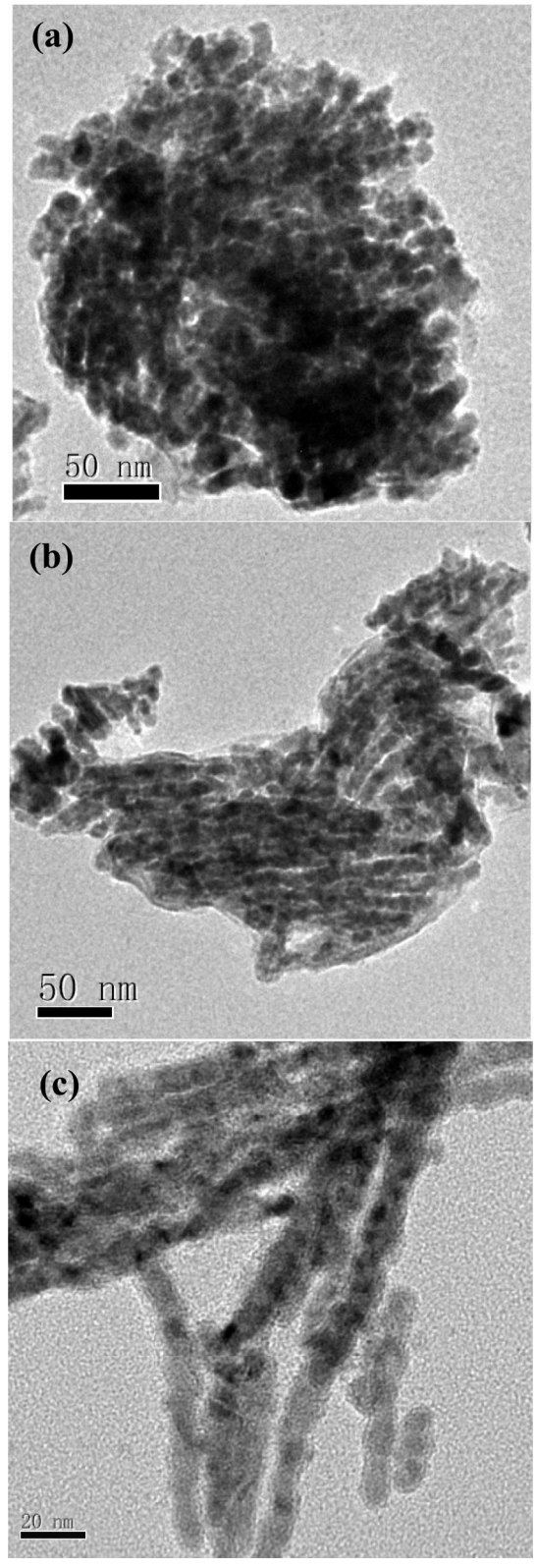


**Figure 9.** Representative TEM morphologies of the (a) Ni-10-2, (b) Ni-20-2, and (c) Ni-30-3 samples.

1), etching the Ni/$NH_2$−SBA-15 precursor for less than 2 days could not completely remove the $NH_2$−SBA-15 template. However, a very long etching time (>3 days) could reduce the ordering degree of Ni nanowires (see Figure 9c), possibly because of the damage to the Ni nanopegs. Meanwhile, low-angle XRD pattern (Figure 10a) and $N_2$ adsorption/desorption isotherms (panels b and c in Figure 10) of Ni-30-1 and Ni-30-3 indicate the long-range structural order of these samples, although the diffraction peak intensity and the nitrogen uptake reduce in some degree relative to Ni-30-2 because of the decrease in the ordering degree of the mesoporous structure.

Other structural parameters are summarized in Table 2. Ni/$NH_2$−SBA-15 displays lower $S_{BET}$ and $V_P$ than $NH_2$−SBA-15, obviously because of the filling of Ni nanowires inside

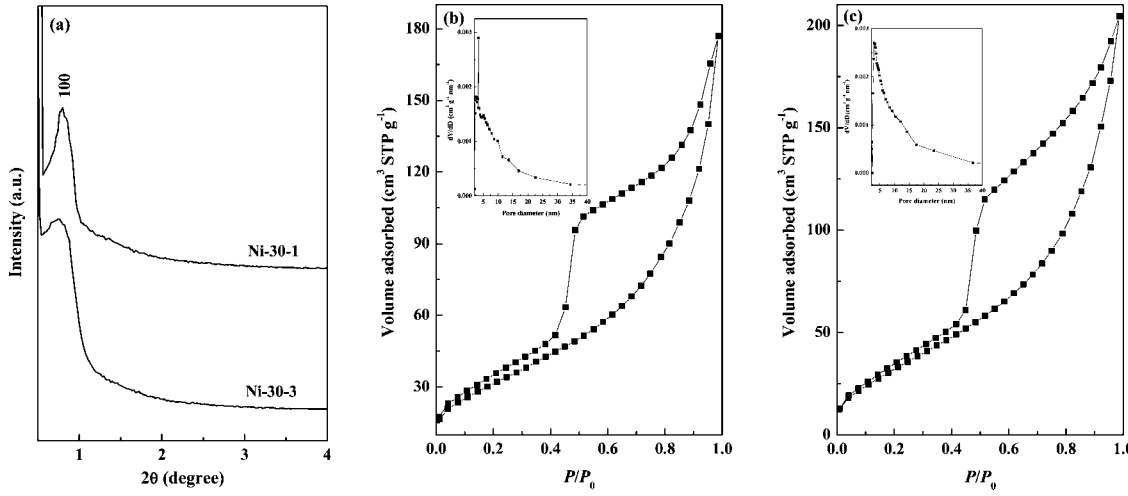


**Figure 10.** (a) Low-angle XRD patterns of the Ni-30-1 and Ni-30-3 samples and adsorption/desorption isotherms of (b) Ni-30-1 and (c) Ni-30-3. The insets are the corresponding pore size distribution curves.

**Table 2. Physical Parameters and Catalytic Performances of Different Ni Samples**[a]

| sample | $S_{BET}$ ($m^2$/g) | $D_P$ (nm) | $V_P$ ($cm^3$/g) | conversion[b](%) | selection [b](%) | yield [b](%) | time [b](min) |
|---|---|---|---|---|---|---|---|
| $NH_2$−SBA-15 | 546 | 8.0 | 0.96 | | | | |
| Ni/$NH_2$−SBA-15 | 307 | 8.0 | 0.43 | | | | |
| Ni-30-1 | 118 | 3.5 | 0.31 | 97.8 | 97.6 | 95.4 | 150 |
| Ni-30-2 | 209 | 3.5 | 0.42 | 97.2 | 97.9 | 95.2 | 90 |
| Ni-30-3 | 151 | 3.2 | 0.33 | 98.5 | 96.3 | 94.9 | 120 |
| Raney Ni | 79 | 3.2 | 0.08 | 97.4 | 95.3 | 92.8 | 320 |

[a] Reaction conditions: Ni-based catalyst containing 0.40 g of Ni, 20 mmol of *p*-CNB, 50 mL of EtOH, $T$ = 353 K, $P_{H_2}$ = 1.0 MPa, stirring rate = 1000 rpm. [b] Values corresponding to the maximum yield of *p*-CAN.

**Scheme 2**

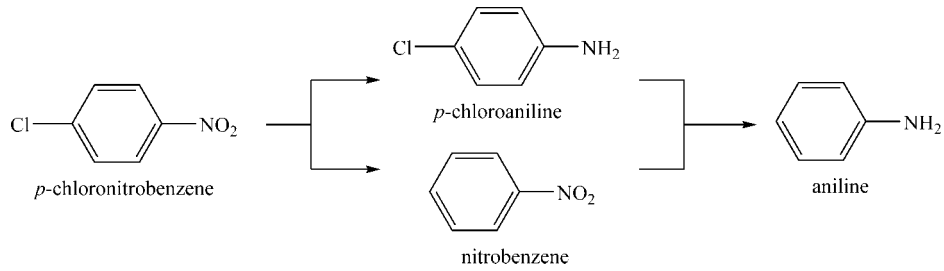


the mesoporous channels.[28] Ni-30−1, Ni-30-2 and Ni-30-3 samples exhibit similar $D_P$ values regardless of the etching time, which further confirms that the pore size is dependent on the pore wall thickness in the $NH_2$−SBA-15 template. Both $S_{BET}$ and $V_P$ increase with the increase of etching time from 1 to 2 days, obviously because of the removal of silica template, leading to the formation of mesopores between Ni nanowires. However, a further increase in etching time to 3 day causes a significant decrease in both $S_{BET}$ and $V_P$ because of partial damage of the mesoporous structure.

Figure 11 shows the concentration change of both the reactant and the products with the reaction time during *p*-CNB hydrogenation over Ni-30-2 and Raney Ni catalysts. Except for the main product *p*-chloroaniline (*p*-CAN), only aniline (AN) and nitrobenzene (NB) are identified as byproducts under the present conditions. Thus, the reaction pathways could be simply described in Scheme 2.[29] Obviously, Ni-30-2 has an induction period, whereas Raney Ni has no induction time. Two possible explanations exist to account for this observation. For Ni-30-2, the surface contaminants (O, P, S, etc.) maybe cover the catalyst surface and thus the activity is lower in the initial period. The catalyst is activated gradually in this period through reducing these oxide species by hydrogen. On the other hand, in general, the rate-determining step is a nucleophilic attack of hydride ion on the nitrogen atom of the nitro group.[30] Accordingly, Ni-30-2 has a lower activity in initial period, taking into account for more time needed for hydrogen to diffuse and adsorb on the catalyst surface, whereas Raney Ni does not have an induction time, because this catalyst contains no surface oxide species and has adsorbed more hydrogen formed during catalyst preparation process.[31] The catalytic parameters are summarized in Table 2. Although Ni-30-2 displays similar selectivity and yield toward *p*-CAN to Raney Ni, it exhibits much higher activity than Raney Ni, corresponding to shorter

(28) Huang, M. H.; Choudrey, A.; Yang, P. D. *Chem. Commun.* **2000**, 1063.
(29) Coq, B.; Tijani, A.; Figuéras, F. *J. Mol. Catal.* **1991**, *68*, 331.
(30) Lu, P.; Toshima, N. *Bull. Chem. Soc. Jpn.* **2000**, *73*, 751.
(31) Hoffer, B. W.; Crezee, E.; Devred, F.; Mooijman, P. R. M.; Sloof, W. G.; Kooyman, P. J.; Van Langeveld, A. D.; Kapteijn, F.; Moulijn, J. A. *Appl. Catal., A* **2003**, *253*, 437.

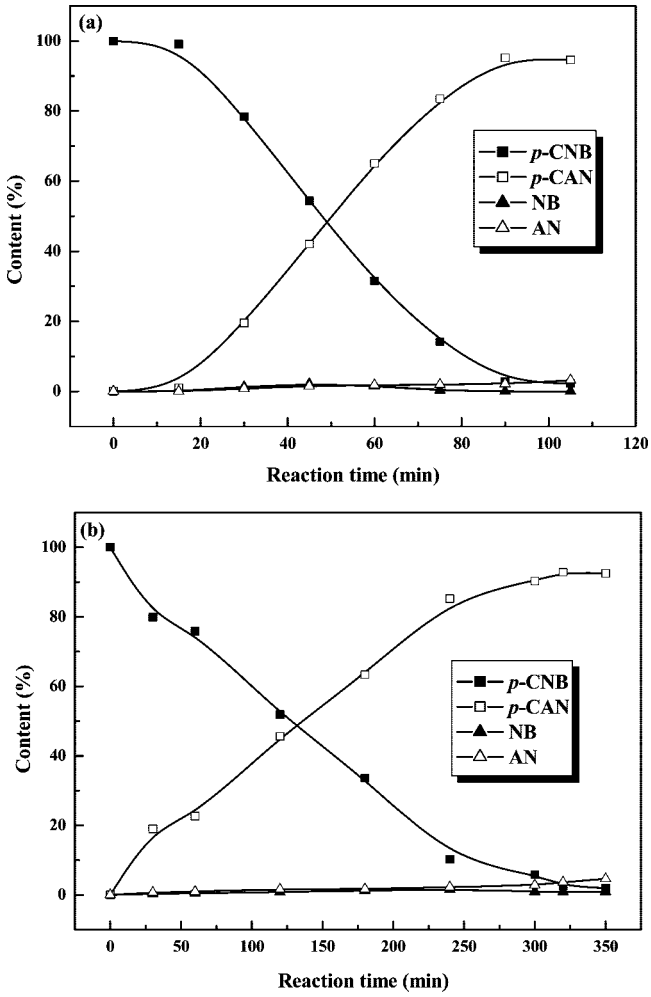


**Figure 11.** Change of the solution composition with the reaction time during *p*-CNB hydrogenation over (a) Ni-30-2 and (b) Raney Ni. Reaction conditions are given in Table 2.

time needed for achieving maximum yield of *p*-CAN. The much higher $S_{BET}$ of mesoporous Ni catalysts could account for their enhanced activities, which might provide more active sites for reactant molecules.[32] Comparing the catalytic performances of Ni-30-1, Ni-30-2, and Ni-30-3 samples, one could find that etching time exhibits no significant influence on the selectivity to *p*-CAN because it could not change the nature and structure of Ni active sites. However, the catalytic activity is strongly dependent on the etching time. Ni-30-1 exhibits much lower activity than Ni-30-2 because the $NH_2$−SBA-15 template that covers the Ni active sites has not been completely removed. Ni-30-3 also displays lower activity than Ni-30-2 because a very long etching time causes partial collapse of the mesoporous structure, leading to lower $S_{BET}$.

The stability of Ni-30-2 catalyst is examined by treating the sample either in $N_2$ flow at 473 K for 12 h or in ethanol solution at 353 K for 10 days. The TEM images (see the Supporting Information, Figure S4) demonstrate that Ni-30-2 is still present in ordered Ni nanowires. Meanwhile, both the low-angle XRD patterns (see the Supporting Information, Figure S5) and the $N_2$ adsorption−desorption isotherms (see the Supporting Information, Figure S6) demonstrate the well preservation of the ordered mesoporous structure. These results confirm that Ni-30-2 is very stable during heating treatment in either the gas phase or the liquid phase, which guarantees the recycling use of Ni-30-2 catalyst.

## Conclusions

In summary, the present work supplies a facile method to prepare ordered mesoporous Ni nanowires by Ni electroless plating on Pd-activated $NH_2$−SBA-15, followed by removing silica template in NaOH solution. Such Ni catalyst exhibits high er activity than Raney Ni in liquid-phase *p*-NB hydrogenation because of the higher surface area. Other metal catalysts could also be prepared on the basis of the present method, which offers more opportunities for designing new and powerful catalysts for industrial applications.

**Acknowledgment.** This work is supported by the National Natural Science Foundation of China (20603023), the 863 Project (2007AA03Z339), the Preliminary 973 Project (2005CCA01100), and Shanghai Government (05QMX1442, T0402, 06JC14093, 07dz22303).

**Supporting Information Available:** Solid-state NMR spectra of $NH_2$−SBA-15, EDX of Ni-30-20, TEM of the Ni prepared using bare SBA-15 as template, and TEM, low-angle XRD, and adsorption/desorption isotherm of Ni-30-20 after thermal treating and ethanol thermal treating (PDF). This material is available free of charge via the Internet at http://pubs.acs.org.

CM800790H

(32) Schmid, G. *Chem. Rev.* **1992**, *92*, 1709.